

MIT Open Access Articles

Wavelet-based motion artifact removal for electrodermal activity

The MIT Faculty has made this article openly available. **Please share** how this access benefits you. Your story matters.

Citation: Weixuan Chen et al. "Wavelet-Based Motion Artifact Removal for Electrodermal Activity." 37th Annual International Conference of the IEEE Engineering in Medicine and Biology Society (EMBC), 25-29 August, 2015, Milan, Italy, IEEE, 2015.

As Published: <http://dx.doi.org/10.1109/EMBC.2015.7319814>

Publisher: Institute of Electrical and Electronics Engineers (IEEE)

Persistent URL: <http://hdl.handle.net/1721.1/110678>

Version: Author's final manuscript: final author's manuscript post peer review, without publisher's formatting or copy editing

Terms of use: Creative Commons Attribution-Noncommercial-Share Alike



Wavelet-Based Motion Artifact Removal for Electrodermal Activity

Weixuan Chen*, Natasha Jaques*, Sara Taylor*, Akane Sano*, Szymon Fedor*, and Rosalind W. Picard*

Abstract—Electrodermal activity (EDA) recording is a powerful, widely used tool for monitoring psychological or physiological arousal. However, analysis of EDA is hampered by its sensitivity to motion artifacts. We propose a method for removing motion artifacts from EDA, measured as skin conductance (SC), using a stationary wavelet transform (SWT). We modeled the wavelet coefficients as a Gaussian mixture distribution corresponding to the underlying skin conductance level (SCL) and skin conductance responses (SCRs). The goodness-of-fit of the model was validated on ambulatory SC data. We evaluated the proposed method in comparison with three previous approaches. Our method achieved a greater reduction of artifacts while retaining motion-artifact-free data.

I. INTRODUCTION

Electrodermal activity (EDA) refers to the changes of the electrical properties of the skin in response to sudomotor innervation [4], which can be recorded as skin conductance (SC) [10]. Since sudomotor innervation is controlled by the sympathetic nervous system (SNS), SC provides a fine measure of SNS activity, and is hence widely used in psychophysiology as an indication of psychological or physiological arousal. Traditional lab-based applications of EDA include the clinical assessment of pain [18], [30], schizophrenia [27], [33] and peripheral neuropathy [26], [31]. Meanwhile, ambulatory measurement of EDA, especially SC, has also found an increasingly wide utilization in studies related to affective phenomena [13], [12], sleep [29], epilepsy [25] and stress [11], [14].

There are several possible sources of artifacts in EDA recordings. While artifacts may result from the recording procedure (e.g. power line noise), these are usually avoidable through exact control of the measurement technique. Motion artifacts, however, are nearly impossible to eliminate entirely, even when subjects are asked to avoid gross body movements. As more and more research adopts ambulatory EDA sensors like Q sensor (Affectiva, Inc.), DTI-2 Wristband (Philips, Inc.) and E4 Wristband (Empatica, Inc.), removing motion artifacts before further statistical treatment becomes even more essential.

Motion artifacts can be caused not only by skin movements beneath the electrodes, but also by muscular activity not directly exerted underneath recording sites [4]. According to [7], unusual steep rises, which are one of the most common artifacts in EDA (see Fig. 1), stem from pressure exerted on the electrodes.

Supported by the MIT Media Lab Consortium and the People Programme (Marie Curie Actions) of the European Union's Seventh Framework Programme FP7/2007-2013/ under REA grant agreement n° 327702

*Affective Computing Group, MIT Media Lab, Massachusetts Institute of Technology, 75 Amherst Street, Cambridge, U.S. {cvx, jaquesn, sataylor, akane, sfedor, picard}@media.mit.edu

Dealing with motion artifacts, an experimenter might choose between correcting or discarding them. Correcting solutions will be more reasonable, if data are short in length or continuity of data is indispensable. There are a few methods previously taken to correct motion artifacts, such as exponential smoothing [14] and other low-pass filters [24], [25], [15]. However, these non-adaptive methods are unable to compensate for artifacts abruptly appearing with much larger intensity than EDA, and the whole time series are filtered indiscriminately, which may distort SC signals without artifacts.

Wavelet transforms offer a more sophisticated denoising method; they have been widely used for removal of artifacts in physiological signals like electroencephalogram (EEG) [17], [35], electrocardiogram (ECG) [8], [1], and photoplethysmogram (PPG) [20]. We expect that most motion artifacts will have different amplitude and duration characteristics than SC responses: these kinds of differences may be better highlighted in the wavelet domain due to a good localization property of the wavelet transform [22]. Furthermore, many adaptive methods have been proposed for wavelet denoising [34], [5], making it easier to reach a balance between artifact attenuation and good signal retention.

Based on all the points above, we present a wavelet-based method with adaptive thresholding for removing motion artifacts from EDA, and evaluate its performance in comparison with previous methods.

II. METHODS

The adaptive denoising procedure used in this paper is briefly given below:

- Utilize stationary wavelet transform (SWT) to expand the contaminated EDA signal into multiple levels of scaling and wavelet coefficients.
- Adaptively select the threshold limit within each time window at each level based on the statistic estimation of the wavelet coefficients' distribution, and employ that on the wavelet coefficients of all levels.
- Apply inverse wavelet transform to the thresholded wavelet coefficients to obtain the denoised EDA signal.

A. Stationary Wavelet Transform

The discrete wavelet transform (DWT) is not time-invariant. Due to this drawback, denoising via the DWT often suffers from additional artifacts like ringing effects in the vicinity of a discontinuity [6]. To address the problem, we used the stationary wavelet transform (SWT) [23], which

is time-invariant and performs no downsampling. Consequently, the length of the sequences at each level is the same as that of the original sequence, which provides better sampling rates in the low frequency bands compared with standard DWT.

SWT decomposition of a signal $y(t)$ results in the scaling (approximation) and wavelet (detail) coefficients:

$$c_{2^j}^{2^j k+p} = \langle y(t), 2^{-j/2} \phi(\frac{t-p}{2^j} - k) \rangle \quad (1)$$

$$d_{2^j}^{2^j k+p} = \langle y(t), 2^{-j/2} \psi(\frac{t-p}{2^j} - k) \rangle \quad (2)$$

where $\phi(t)$ and $\psi(t)$ are the scaling and wavelet functions, j and k amount to the scaling and translation of the wavelet basis, and $p \in 0, \dots, 2^j - 1$ allows for all the possible shifts in a discrete setting. Here we chose $j \in 1, \dots, 8$, which means EDA data were decomposed into 8 levels. An illustrative SC signal was drawn with its 4th level wavelet coefficients and corresponding actigraph in Fig. 1.

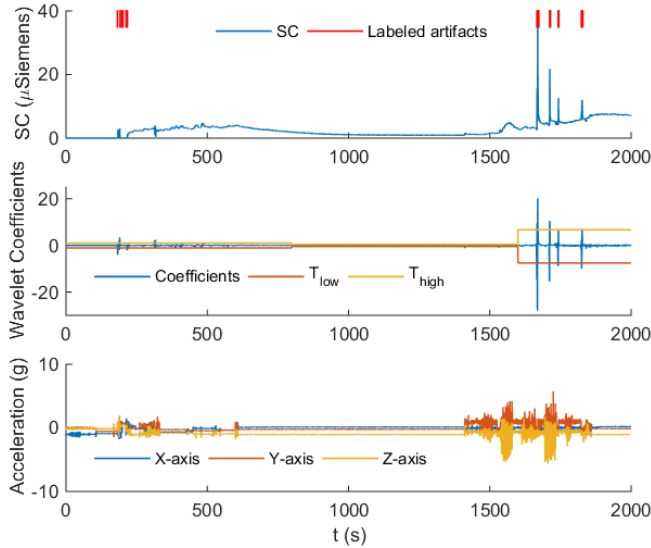


Fig. 1. SC signal with motion artifacts labeled by two expert EDA researchers; Wavelet coefficients with adaptive thresholds; Actigraph in three axes.

B. Wavelet Coefficient Model

Distribution of wavelet coefficients can be modeled as a mixture of two Gaussians [2], [5]. One Gaussian component describes coefficients centered around zero, and the other describes those spread out at larger values. This model fits the characteristics of SC signals well. Time series of SC can be characterized by a slowly varying tonic activity (i.e., skin conductance level; SCL) and a fast varying phasic activity (i.e., skin conductance responses; SCRs) [3]. After high-pass filtering inside the SWT, the wavelet coefficients of SCL and SCRs will both have mean values around zero. A typical histogram of the wavelet coefficients of an SC signal is shown in Fig. 2, with a fitted model of two mixed Gaussians superimposed. As is illustrated in the histogram, the Gaussian with smaller variance corresponds to the wavelet coefficients

of SCL, while the Gaussian with larger variance corresponds to the wavelet coefficients of SCRs. Apart from the two distributions, there are a few very large coefficients in the histogram, which are motion artifacts we wanted to remove.

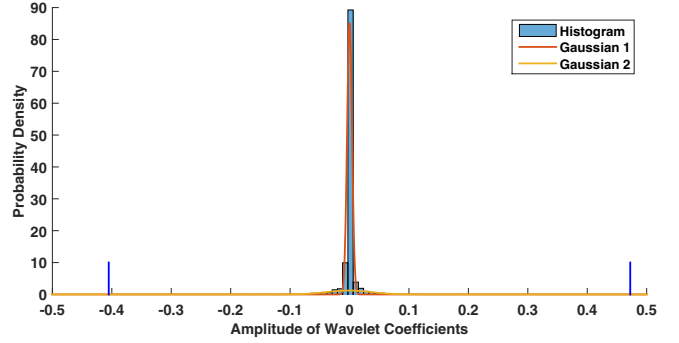


Fig. 2. A typical histogram of the wavelet coefficients of an SC signal with a fitted model of two mixed Gaussians superimposed. The two blue vertical lines represent the minimum and maximum values of the histogram.

In summary, the wavelet coefficients of an observed SC signal $y(t)$ can be written as

$$d_{2^j}^{2^j k+p} = \tilde{d}_{2^j}^{2^j k+p} + \varepsilon_{2^j}^{2^j k+p} \quad (3)$$

$$\tilde{d}_{2^j}^{2^j k+p} \sim \gamma_j N(0, \sigma_j^2) + (1 - \gamma_j) N(0, c_j^2 \sigma_j^2) \quad (4)$$

where ε is the wavelet coefficients of motion artifacts, \tilde{d} is the wavelet coefficients of valid SC, γ_j is the mixture parameter, and σ_j^2 and $c_j^2 \sigma_j^2$ are the variances of the two Gaussians. Assuming ε takes up a very small proportion, from the wavelet coefficients of the original signal d , γ_j , σ_j and c_j can be estimated for each level j using an Expectation Maximization (EM) algorithm [21].

Once the Gaussian mixture model is established for \tilde{d} , two threshold limits can be computed to remove ε . Assume the proportion of ε in d is δ (the artifact proportion). For any given coefficient $d_{2^j}^{2^j k+p}$, if the probability of observing values smaller or larger than $d_{2^j}^{2^j k+p}$ is less than $\delta/2$, we can conclude that the coefficient does not belong to the valid SC and should be a result of motion artifacts. Therefore,

$$\Phi(T_{low}) = 1 - \Phi(T_{high}) = \delta/2 \quad (5)$$

where Φ is the cumulative distribution function (CDF) of the Gaussian mixture distribution, and T_{low} and T_{high} are the thresholds. Finally, motion artifacts can be removed from the wavelet coefficients using the following scheme:

$$d_{2^j}^{2^j k+p} = \begin{cases} d_{2^j}^{2^j k+p} & \text{if } T_{low} < d_{2^j}^{2^j k+p} < T_{high} \\ 0 & \text{otherwise} \end{cases} \quad (6)$$

In order to test the goodness-of-fit of the model introduced above, a Q-Q plot was drawn for the thresholded wavelet coefficients of an ambulatory SC time series in Fig. 3. This plot shows empirical quantiles against theoretical quantiles. When the distribution of the data has the same shape as the reference distribution, the points in the QQ plot will

approximately lie on the line $y = x$. Fig. 3 indicates that the wavelet coefficients after thresholding are described very well by a Gaussian mixture model.

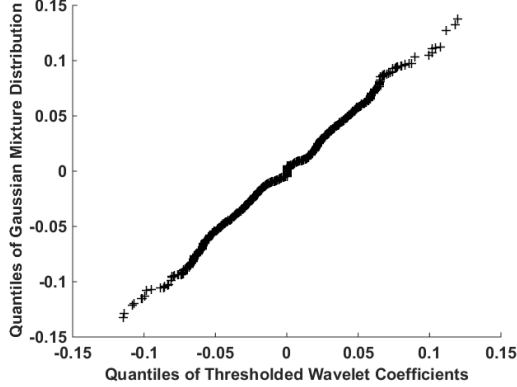


Fig. 3. Q-Q plot of sample wavelet coefficients after thresholding versus a fitted Gaussian mixture distribution.

C. Adaptive Thresholding

As the presence and amplitude of SCRs in SC data fluctuate with the variation of arousal over time, it is not accurate to model a whole level of wavelet coefficients as a single Gaussian mixture distribution. Therefore, (4) was modified to

$$\hat{d}_{2j}^{j,k+p} \sim \gamma_{j,k} N(0, \sigma_{j,k}^2) + (1 - \gamma_{j,k}) N(0, c_{j,k}^2 \sigma_{j,k}^2) \quad (7)$$

where $\gamma_{j,k}$, $\sigma_{j,k}$ and $c_{j,k}$ all change over time. To adaptively estimate these parameters, every level of wavelet coefficients was divided into multiple time windows with a length of L , and thresholds in (5) were calculated independently for each time window. As is shown in Fig. 1, this adaptive thresholding method enabled the denoising thresholds to be better estimated when statistical parameters with respect to SCL and SCRs varied with time. In time windows where SCRs have small amplitudes, the absolute values of the thresholds will also be small.

III. RESULTS

A. Data Collection

EDA data containing motion artifacts was obtained from a previous study [9], in which 32 subjects completed physical, cognitive and emotional tasks while wearing Q sensors on both wrists. During each trial, the Q sensors recorded SC, actigraphs (acceleration) and body temperature at a sampling frequency of 8 Hz for approximately 80 minutes. After discarding 3 incomplete records due to disconnected memory cards, there were in total 61 records of data. Two expert EDA researchers reviewed these data to manually label portions of the SC signals as containing motion artifacts (see Fig. 1).

B. Implementation of Denoising Methods

We applied our wavelet-based motion artifact removal to each SC time series in the dataset. The Haar wavelet was used as the mother wavelet, because of its advantage for

detecting edges and sharp changes [32], commonly seen in motion artifacts. The two tuning parameters of the algorithm, artifact proportion δ and time window length L , were set to be 0.01 and 400 seconds respectively.

Three previous methods removing motion artifacts from EDA were also implemented for comparison. They are 1024-point low-pass Hamming filtering (cutoff frequency = 3 Hz) [24], [25], Hanning filtering with a 1 second window [15] and exponential smoothing ($\alpha = 0.8$) [14].

C. Evaluation

In Fig. 4, a 3000-second excerpt of EDA was visualized with output signals denoised by different methods. The spike artifacts caused by motion in the original signal were only fully removed by our wavelet thresholding algorithm.

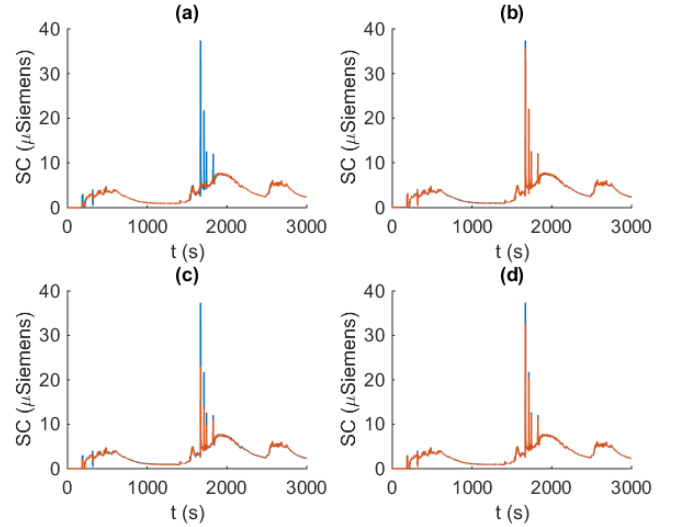


Fig. 4. Original EDA (blue lines) and denoised signals (red lines) processed by (a) wavelet thresholding, (b) Hamming filtering, (c) Hanning filtering and (d) exponential smoothing.

To quantitatively evaluate and compare the performance of all the methods, we used artifact power attenuation (APA) and normalized mean-squared error (NMSE) [22] as criteria. APA is defined as

$$APA_m = 10 \log_{10} \frac{\sum_{n \in A_m} \text{Var}[y(n)]}{\sum_{n \in A_m} \text{Var}[\tilde{y}(n)]} \quad (8)$$

where A_m is the artifact time interval labeled by experts for the m -th artifact, $\text{Var}(\cdot)$ is the variance of a signal, $y(n)$ is the original signal, and $\tilde{y}(n)$ is the processed signal. This measure is basically the ratio of artifact energy before and after removal in dB, which quantifies the intensity of artifact attenuation.

NMSE is defined as

$$NMSE = 10 \log_{10} \frac{\sum_{n \notin A_m} [y(n) - \bar{y}(n)]^2}{\sum_{n \notin A_m} [\tilde{y}(n) - \bar{y}(n)]^2} \quad (9)$$

where $\bar{y}(n)$ is the mean value of $y(n)$. The NMSE is calculated only for motion-artifact-free segments, which are extracted by looking at the corresponding actigraphs. When

acceleration derivatives in three axes were all continuously lower than 0.02g (0.017g is the quantification unit of the accelerometers in Q sensors) for more than 1 minute, the simultaneous SC data would be regarded as motion-artifact-free. The measure NMSE shows how much distortion has been introduced to these portions of the signals.

The median of APA and NMSE across all records of data for each evaluated method are presented in Table I. It is clear that the artifact attenuation ability of our wavelet-based method is much better than those of all the other methods, while their distortion of artifact-free data are basically at the same level. In terms of APA, the Hanning filtering method is the closest to our method, but its NMSE is also the worst.

TABLE I

MEDIAN OF NMSE AND APA (IN dB) FOR THE EVALUATED METHODS.

Methods	Wavelet Thresholding	Hamming Filtering	Hanning Filtering	Exponential Smoothing
APA	6.3233	0.0233	1.2539	0.2559
NMSE	-54.4229	-54.4175	-48.1641	-57.5739

IV. DISCUSSION AND CONCLUSION

Compared with previous approaches, our wavelet thresholding technique achieved much larger intensity of artifact attenuation while retaining clean signals as well as the other methods. It can be easily applied to any future research involving EDA data analysis.

Our method was based on an additive model for interference caused by motion. This assumption of the additive noise model is commonly made and justified in previous studies dealing with motion artifacts [19], [28], [16].

In the future, we hope to quantitatively discuss the two tuning parameters of our algorithm, the artifact proportion δ and the time window length L in relation to performance and give suggestions on their selection. In addition, we would like to examine the potential utility of the Coiflet 3 wavelet [17], [35], since it resembles the shape of a typical motion artifact.

REFERENCES

- [1] M. Alfaouri and K. Daqrouq. ECG signal denoising by wavelet transform thresholding. *Amer. J. of appl. sci.*, 5(3):276–281, 2008.
- [2] A. Antoniadis et al. Wavelet estimators in nonparametric regression: a comparative simulation study. *J. of Stat. Software*, 6(6):1–83, 2001.
- [3] M. Benedek and C. Kaernbach. A continuous measure of phasic electrodermal activity. *J. of neurosci. methods*, 190(1):80–91, 2010.
- [4] W. Boucsein. *Electrodermal activity*. Springer Science & Business Media, 2012.
- [5] H. A. Chipman et al. Adaptive Bayesian Wavelet Shrinkage. *J. of the American Statistical Association*, 92(440):1413–1421, 1997.
- [6] R. R. Coifman and D. L. Donoho. *Translation-invariant de-noising*. Springer, 1995.
- [7] R. Edelberg. Electrical properties of the skin. *Methods in psychophysiology*, pages 1–53, 1967.
- [8] E. Ercelebi. Electrocardiogram signals de-noising using lifting-based discrete wavelet transform. *Computers in Biology and Medicine*, 34(6):479–493, 2004.
- [9] S. Fedor and R. Picard. Ambulatory EDA: Comparison of bilateral forearm and calf locations. In *Society for Psychophysiological Research (SPR)*, Atlanta, 2014.
- [10] D. C. Fowles et al. Publication recommendations for electrodermal measurements. *Psychophysiology*, 18(3):232–239, 1981.

- [11] J. Healey and R. Picard. Detecting stress during real-world driving tasks using physiological sensors. *IEEE Trans. Intell. Transp. Syst.*, 6(2):156–166, June 2005.
- [12] E. Hedman. The Frustration of Learning Monopoly : The Emotional Tension of Entering a New Game Encounter. In *The Ethnographic Praxis in Industry Conference, Boulder*, pages 18–21, 2011.
- [13] E. Hedman et al. Measuring autonomic arousal during therapy. In *Proceedings of 8th International Design and Emotion Conference, London*, 2012.
- [14] J. Hernandez et al. Call center stress recognition with person-specific models. *Proceedings of the Affective Computing and Intelligent Interaction, Memphis*, 2011.
- [15] J. Hernandez et al. Using electrodermal activity to recognize ease of engagement in children during social interactions. In *Int. Conf. on Ubiquitous Computing, Seattle*, 2014.
- [16] M. Izzetoglu et al. Motion artifact cancellation in NIR spectroscopy using Wiener filtering. *IEEE Trans. Biomed. Eng.*, 52(5):934–938, 2005.
- [17] V. Krishnaveni et al. Removal of ocular artifacts from EEG using adaptive thresholding of wavelet coefficients. *J. of neural engineering*, 3(4):338–346, 2006.
- [18] T. Ledowski et al. The assessment of postoperative pain by monitoring skin conductance: results of a prospective study. *Anaesthesia*, 62(10):989–993, 2007.
- [19] B. Lee et al. Improved elimination of motion artifacts from a photoplethysmographic signal using a Kalman smoother with simultaneous accelerometry. *Physiological measurement*, 31(12):1585, 2010.
- [20] C. Lee and Y. Zhang. Reduction of motion artifacts from photoplethysmographic recordings using a wavelet denoising approach. *IEEE EMBS Asian-Pacific Conference on Biomedical Engineering, 2003*, pages 194–195, 2003.
- [21] G. McLachlan and D. Peel. *Finite mixture models*. John Wiley & Sons, 2004.
- [22] B. Molavi and G. A. Dumont. Wavelet-based motion artifact removal for functional near-infrared spectroscopy. *Physiological Measurement*, 33(2):259–270, 2012.
- [23] G. P. Nason and B. W. Silverman. The stationary wavelet transform and some statistical applications. In *Wavelets and statistics*, pages 281–299. Springer, 1995.
- [24] M. Poh et al. A Wearable Sensor for Unobtrusive, Long-Term Assessment of Electrodermal Activity. *IEEE Trans. Biomed. Eng.*, 57(5):1243–1252, 2010.
- [25] M. Poh et al. Continuous monitoring of electrodermal activity during epileptic seizures using a wearable sensor. In *2010 Annual Int. Conf. of the IEEE Engineering in Medicine and Biology Society (EMBC)*, pages 4415–4418, 2010.
- [26] A. Polo et al. Painless fractures and thermoregulation disturbances in sensory-autonomic neuropathy: electrophysiological abnormalities and sural nerve biopsy. *Neuropediatrics*, 31(3):148–150, 2000.
- [27] A. Raine et al. Skin-conductance orienting deficits and increased alcoholism in schizotypal criminals. *J. of abnormal psychology*, 108(2):299, 1999.
- [28] F. C. Robertson et al. Motion artifact removal for functional near infrared spectroscopy: a comparison of methods. *IEEE Trans. Biomed. Eng.*, 57(6):1377–1387, 2010.
- [29] A. Sano et al. Quantitative analysis of wrist electrodermal activity during sleep. *Int. J. of Psychophysiology*, 94(3):382–389, 2014.
- [30] H. Storm. Changes in skin conductance as a tool to monitor nociceptive stimulation and pain. *Current Opinion in Anesthesiology*, 21(6):796–804, 2008.
- [31] K. Torigoe et al. Sympathetic skin response in diabetic children: Do diabetic children have diabetic neuropathy? *Pediatrics international*, 41(6):631–636, 1999.
- [32] Y. Xu et al. Wavelet transform domain filters: a spatially selective noise filtration technique. *IEEE Trans. Image Process.*, 3(6):747–758, 1994.
- [33] K. Yamamoto and O. Hornykiewicz. Proposal for a noradrenaline hypothesis of schizophrenia. *Progress in Neuro-Psychopharmacology and Biological Psychiatry*, 28(5):913–922, 2004.
- [34] X. P. Zhang and M. D. Desai. Adaptive denoising based on SURE risk. *IEEE Signal Process. Lett.*, 5(10):265–267, 1998.
- [35] T. Zikov et al. A wavelet based de-noising technique for ocular artifact correction of the electroencephalogram. In *Proceedings of the Second Joint EMBS/BMES Conference, Houston*, pages 98–105, 2002.